Available online at www.sciencedirect.com
ScienceDirect
Construction and Building Materials 21 (2007) 827–838
Construction and Building MATERIALS
www.elsevier.com/locate/conbuildmat

# Behaviour of FRP-jacketed circular steel tubes and cylindrical shells under axial compression

J.G. Teng *, Y.M. Hu

*Department of Civil and Structural Engineering, The Hong Kong Polytechnic University, Hong Kong, China*

Received 22 February 2006; received in revised form 24 May 2006; accepted 19 June 2006
Available online 1 September 2006

**Abstract**

Fibre-reinforced polymer (FRP) jackets have been widely used to confine reinforced concrete (RC) columns for enhancement in both strength and ductility. This paper presents the results of a recent study in which the benefit of FRP confinement of hollow steel tubes was explored. Axial compression tests on FRP-confined steel tubes are first described. Finite element modelling of these tests is next discussed. Both the test and the numerical results show that FRP jacketing is a very promising technique for the retrofit and strengthening of circular hollow steel tubes. In addition, finite element results for FRP-jacketed thin cylindrical shells under combined axial compression and internal pressure are presented to show that FRP jacketing is also an effective strengthening method for such shells failing by elephant's foot collapse near the base.


*Keywords:* Steel tubes; Cylindrical shells; FRP jacketing; Strengthening; Retrofit

## 1. Introduction

Over the past decade, fibre-reinforced polymer (FRP) composites have been widely used in the strengthening of concrete structures [1,2]. More recently, the use of FRP to strengthen metallic structures has also attracted a significant amount of attention [3], but this work has generally been limited to the strengthening of metallic beams by the bonding of FRP laminates. The present paper is concerned with the performance enhancement of circular hollow steel tubes with FRP jacketing.

Circular hollow steel tubes are widely used as columns in many structural systems and a common failure mode of such tubes when subjected to axial compression and bending is local buckling near a column end. For example, hollow steel tubes are often used as bridge piers and such bridge piers suffered extensive damage and even collapses during the 1995 Hyogoken-nanbu earthquake [4]. Fig. 1a shows a local buckling failure mode at the base of a steel bridge pier and the repair of the pier by the addition of welded vertical stiffeners. Such local buckling is often referred to as elephant's foot buckling. In typical circular tubular members, elephant's foot buckling appears after yielding and the appearance of this inelastic local buckling mode normally signifies the exhaustion of the load carrying capacity and/or the end of ductile response. The latter is of particular importance in seismic design, as the ductility and energy absorption capacity of the column dictates its seismic resistance. A number of methods have been proposed for the seismic retrofit of hollow steel tubes as bridge piers where enhancement of ductility without a significant strength increase is preferred, but each method suffers from some limitations [5].

Xiao [6] and Xiao et al. [7] recently explored the use of FRP jackets for the confinement of the critical regions of concrete-filled steel tubes. Although his work appears to be directed at new construction, the same concept can be employed in the retrofit of columns. In such columns, the

* Corresponding author. Tel.: +86 852 2766 6012; fax: +86 852 2334 6389.
*E-mail address:* cejgteng@polyu.edu.hk (J.G. Teng).

0950-0618/$ - see front matter © 2006 Elsevier Ltd. All rights reserved.
doi:10.1016/j.conbuildmat.2006.06.016

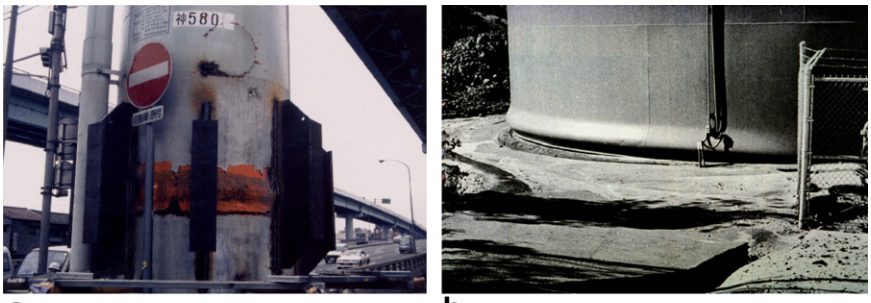


Fig. 1. Elephant's foot buckling in a steel tube or shell (Courtesy of Dr. H.B. Ge, Nagoya University & Prof. J.M. Rotter, Edinburgh University). (a) Failure near the base of a steel tube. (b) Failure at the base of a liquid storage tank.

inward buckling deformation of the steel tube is prevented by the concrete core while the outward buckling deformation is prevented by the FRP jacket. FRP jacketing therefore provides a very effective means of suppressing local buckling failures at columns ends. Two research groups have recently explored the FRP jacketing of hollow steel tubes independently. Teng and Hu [8] extended Xiao's concept to circular hollow steel tubes and showed that even in hollow tubes where inward local buckling is not prevented, FRP jacketing provides a simple and effective method for the ductility enhancement and hence seismic retrofit of such columns. During the preparation of the present paper, the authors became aware of work by Nishino and Furukawa [9] undertaken in Japan, which explored the same technique for hollow steel tubes independently.

The idea of FRP jacketing of circular steel tubes can be extended to circular cylindrical shells (or even general shells of revolution) if the elephant's foot buckling mode is the critical failure mode. It is well known that large thin steel cylindrical shells such as liquid storage tanks and steel silos for storage of bulk solids may fail in the elephant's foot buckling mode at the base (Fig. 1b) when subject to the combined action of axial compression and internal pressure [10,11]. Many such failures have been observed during earthquakes. In addition to the base of a shell, the elephant's foot failure mode can also occur at a discontinuity that leads to local bending, such as at a lap joint [12]. For such steel cylindrical shells, FRP confinement appears to be an effective method of retrofit and may also be considered in new tank/silo designs.

This paper presents the results of a recent study in which the benefit of FRP confinement of hollow steel tubes under axial compression was examined. Axial compression tests on FRP-confined steel tubes, which were first presented in Ref. [8], are described. Finite element modelling of these tests is next discussed. Both the test and the numerical results show that FRP jacketing is a very promising technique for the retrofit and strengthening of circular hollow steel tubes. In addition, finite element results for FRP-jacketed thin cylindrical shells under combined axial compression and internal pressure are presented to show that FRP jacketing is also an effective strengthening method for such shells failing by elephant's foot collapse near the base.

## 2. Experiments

### 2.1. Specimens

In order to demonstrate the effect of FRP confinement on steel tubes, four steel tubes with or without a glass FRP (GFRP) jacket were tested at The Hong Kong Polytechnic University. The four tubes were cut from a single long tube and their details are shown in Table 1. GFRP was used instead of carbon FRP (CFRP) in these tests as GFRP possesses a larger ultimate tensile strain and was expected to lead to greater enhancement of the ductility of the tube. The four tubes are named respectively, ST-F0, ST-F1, ST-F2 and ST-F3, with the last number indicating the number of plies of the FRP jacket (Table 1). The GFRP jacket was formed in a wet lay-up process, and each ply consisted of a single lap of a glass fibre sheet impregnated with epoxy resin. A continuous glass fibre sheet was wrapped around the steel tube to form a jacket with the required number of plies, with the finishing end of the fibre sheet overlapping its starting end by 150 mm to ensure circumferential continuity. Before the wrapping of GFRP, the surface of the steel tube was cleaned using alcohol.

Three steel coupon tests were conducted according to BS18 [13] to determine the tensile properties of the steel. The tensile test specimens were cut from a single steel tube which in turn was cut from the same long tube as the tube specimens for compression tests. The average values of the elastic modulus, yield stress, ultimate strength, and elongation after fracture from these tensile tests were 201.0 GPa, 333.6 MPa, 370.0 MPa and 0.347, respectively.

Five tensile tests according to ASTM3039 [14] were also conducted for the GFRP material which had a nominal thickness of 0.17 mm per ply. The average values of the elastic modulus and tensile strength from these tests, calculated

Table 1
Specimen details

| Tube specimen | ST-F0 | ST-F1 | ST-F2 | ST-F3 |
|---|---|---|---|---|
| Outer diameter (mm) | 165 | 166 | 165 | 165 |
| Length (mm) | 450 | 450 | 450 | 450 |
| Tube thickness (mm) | 4.2 | 4.2 | 4.2 | 4.2 |
| FRP jacket thickness | NA | One ply | Two plies | Three plies |

on the basis of the nominal ply thickness of 0.17 mm, were 80.1 GPa and 1825.5 MPa, respectively, leading to an ultimate tensile strain of 0.0228.

### 2.2. Instrumentation and loading

For the bare steel tube, four unidirectional strain gauges with a gauge length of 8 mm were installed at the mid-height to measure axial strains. For each FRP-confined steel tube, four bidirectional strain gauges with a gauge length of 20 mm were installed at the mid-height of the FRP jacket. The layout of strain gauges is shown in Fig. 2 for each FRP-confined specimen. The compression tests were all conducted using an MTS machine with displacement control (Fig. 3). The loading rate was 0.5 mm/min. The total shortening of the steel tube was taken to be the same as the relative movement between the two loading platens recorded by the MTS machine. Some steel block spacers existed between the steel tube and the loading platens (Fig. 3), but their deformation was small and was ignored.

### 2.3. Test observations and results

The failure mode of the bare steel tube was outward buckling around the circumference. This local buckling mode near the tube end, widely known as the elephant's foot buckling mode (Fig. 4), is normally found in steel tubes whose diameter-to-thickness ratio is relatively small. Two load–axial strain curves of the steel tube are shown in Fig. 5. One of the curves is for the average strain from the four strain gauges at the mid-height of the steel tube, while the other curve is for the nominal axial strain, which is equal to the average total axial shortening divided by the height of the steel tube. The four strain gauges recorded axial strains very close to each other until unloading took place. During the post-buckling regime, the axial strain at the mid-height reduces as the load reduces, but the nominal axial strain steadily increases. This means that load–strain curves in the post-buckling regime from strain gauge readings depend strongly on strain gauge locations and do not

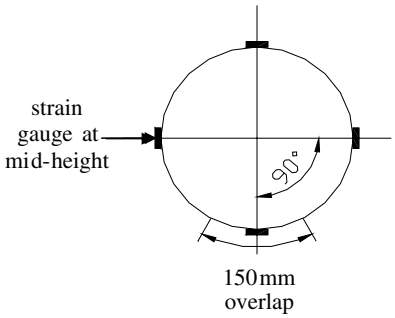


Fig. 2. Layout of strain gauges for FRP-confined steel tube specimens.

Fig. 3. Test set-up.

Fig. 4. Bare steel tube after compression test.

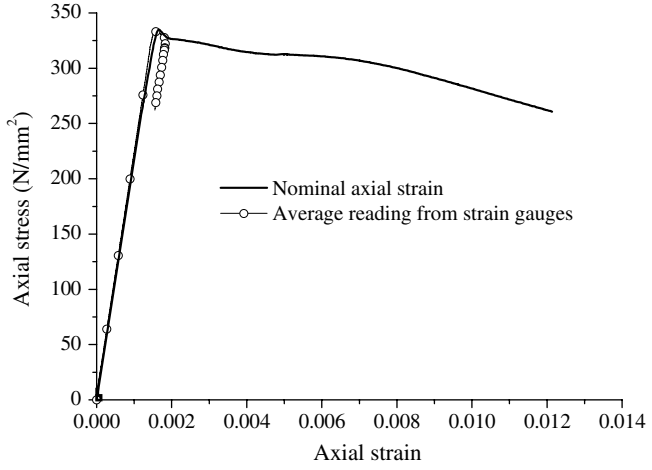


Fig. 5. Experimental axial stress–axial strain curves of the bare steel tube.

reflect the global behaviour of the tube (e.g. the energy absorption capacity of the tube). Therefore, from here onwards, only load–axial shortening curves are shown.

The three FRP-confined steel tubes after failure are shown in Fig. 6. Readings from strain gauges at the mid-height indicated that the axial load was well centred in all three tests. The load–axial shortening curves of these three specimens together with that of the bare steel tube are shown in Fig. 7. While the load–axial shortening curve of the bare steel tube features a descending branch immediately after the linearly ascending branch, those of the three FRP-confined tubes all feature a long and slowly ascending branch before reaching the peak load, showing great ductility. Fig. 7 shows that the tube confined with a single-ply FRP jacket is almost as ductile as those with a two-ply or a three-ply jacket. For practical applications, methods need to be developed to achieve optimum designs of FRP jackets.

In the steel tube with a single-ply FRP jacket, failure involved outward local buckling deformations near the ends, causing the FRP jacket to eventually rupture due to hoop tension. It should be noted that in these steel tubes, local rupture of the FRP jacket at one or more locations did not affect the load–axial shortening behaviour significantly, so it is not possible to identify from a load–axial shortening curve when local rupture of FRP was first reached. Some inward buckling deformations also developed in this specimen, but the outward deformations dominated the behaviour. In the tube with a two-ply FRP jacket, the FRP jacket also ruptured near one of the ends due to the expanding local buckling deformations but inward buckling deformations became more important in this tube. When a three-ply FRP jacket was used, local rupture of the FRP jacket did not occur and failure was dominated by inward buckling deformations away from the two ends. It is obvious that in such steel tubes, as the thickness


Fig. 6. FRP-confined steel tubes after compression test.

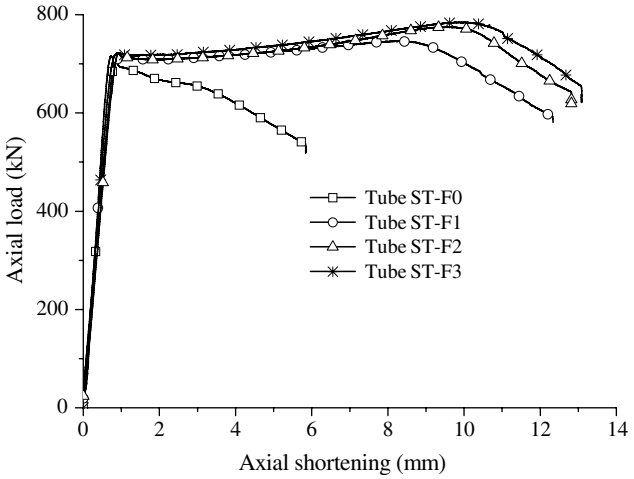


Fig. 7. Experimental load–axial shortening curves of all four steel tubes.

of the FRP jacket increases, the outward buckling deformations near the ends are increasingly restrained, making inward buckling deformations away from the ends increasingly more important. Since the FRP jacket offers little resistance to inward buckling deformations, once the behavior is dominated by inward bucking, the use of a thicker jacket leads to little additional benefit (Fig. 7).

Key test results are summarized in Table 2, where $P_{co}$ is the yield load defined as the yield stress of the steel from tensile coupon tests times the cross-sectional area of the steel tube (taking the diameters of all specimens to be 160.8 mm) and $P_u$ is the ultimate load obtained from the compression tests. $\Delta_{co}$ is the axial shortening of the bare steel tube at peak load from the bare steel tube compression test, while $\Delta_u$ is the axial shortening of an FRP-confined steel tube at peak load. It can be found that both $P_u$ and $\Delta_u$ increase with the thickness of the FRP jacket.

The confinement effectiveness of the FRP jacket can be gauged by examining the degrees of enhancement in the ultimate load and the axial shortening at peak load. As seen in Table 2, the ultimate load of the steel tube was enhanced by 5–10% by FRP jackets of different thicknesses. The ultimate load increases with the thickness of the FRP jacket, although this increase is generally very limited. Table 2 and Fig. 7 both show that the ductility of the steel tube was greatly enhanced by FRP confinement. The axial shortening at peak load is enhanced by around 10 times through FRP confinement. It is worth noting that

Table 2
Summary of test results

| Specimen | ST-F0 | ST-F1 | ST-F2 | ST-F3 |
|---|---|---|---|---|
| $P_{co}$ (kN) | 707.4 | | | |
| $P_u$ (kN) | 717.5 | 740.4 | 771.0 | 782.2 |
| $P_u/P_{co}$ | 1.01 | 1.05 | 1.09 | 1.10 |
| $\Delta_{co}$ (mm) | 0.936 | | | |
| $\Delta_u$ (mm) | 0.936 | 8.662 | 9.691 | 10.114 |
| $\Delta_u/\Delta_{co}$ | 1.00 | 9.25 | 10.35 | 10.80 |

FRP confinement of circular hollow steel tubes leads to great increase in ductility with very limited increases in strength, a feature that is highly desirable in the seismic retrofit of structures. Therefore, FRP jacketing appears to be a very promising technique for the seismic retrofit of circular steel tubular columns.

## 3. Finite element modelling of the bare steel tube

### 3.1. General

The general-purpose finite element software package ABAQUS [15] was employed to simulate the test tubes in this study. To model these tests, both geometric and material nonlinearities were considered and the nonlinear load–deformation path was followed by the arc-length method. Symmetry conditions were not exploited so that the deformation pattern was not restricted by imposing such conditions. The modelling of the bare steel tube is first examined in this section. As for the test results, the finite element results are also reported in terms of the load–axial shortening curves.

The steel tube was modelled using element S4R. Element S4R is a 4-node doubly curved general-purpose shell element with the effect of transverse shear deformation included. Each node has six degrees of freedom (three translations and three rotations). Nine integration points were adopted for integration across the thickness. A mesh convergence study was conducted, leading to a uniform mesh of 5 mm × 10 mm elements for the steel tube, which was found to provide accurate predictions. The longer side of the element lies in the circumferential direction, as the number of waves of the deformations of the tube in the circumferential direction is generally small. The stress–strain curve for the steel adopted in the finite element model is shown in Fig. 8. This curve is based on the average values of the yield stress and the elastic modulus, and the shape of its strain-hardening part is based on test curve 1 shown in Fig. 8.

Based on numerical results obtained with the finite element model, the final finite element model arrived to include the following two features, the need of which is not apparent in a straightforward finite element modelling exercise: (a) the two ends are fully fixed except that the axial displacement of the top end is left unrestrained to allow the application of axial loading; (b) a small geometric imperfection is included to guide the finite element model into a deformation pattern similar to that found in the test. The rationale for these choices is explained below, where the finite element results are from a finite element model with the above features included unless otherwise specified.

### 3.2. Boundary conditions

In the experiment, the steel tube was in contact with stiff loading plates at the two ends (Fig. 3). While this support condition may appear to be close to a simply-supported condition, the numerical comparison shown in Fig. 9 indicates that a clamped support condition for the two ends leads to much closer predictions of the test results. Furthermore, the deformed shape of the tube from the finite element model with clamped ends is also in much close agreement with that from the test (Fig. 10). Therefore, the clamped end condition is more appropriate for this tube. This means that the tube wall was sufficiently thick that the loading plates in contact provided significant restraints at the ends against meridional rotations.

### 3.3. Geometric imperfection

For a perfect steel tube under axial compression, the two ends are each expected to develop a local elephant's foot buckle. In an experiment, this generally does not occur due to small geometric and material imperfections (Fig. 4). Therefore, for the finite element analysis to capture the experimental behaviour realistically, a geometric imperfection was included in the finite element model. In

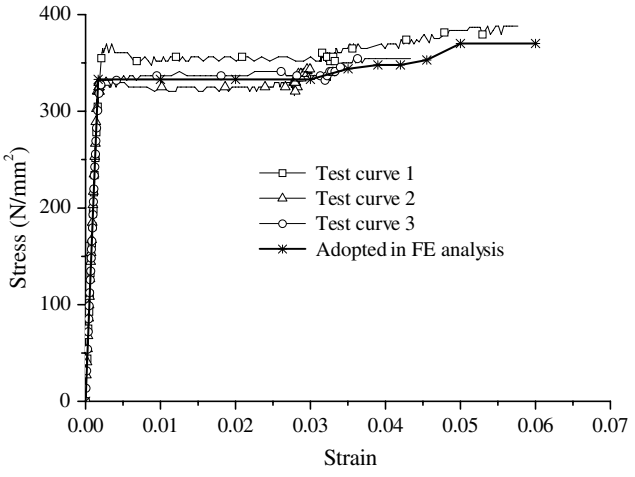


Fig. 8. Tensile stress–strain curves of steel.

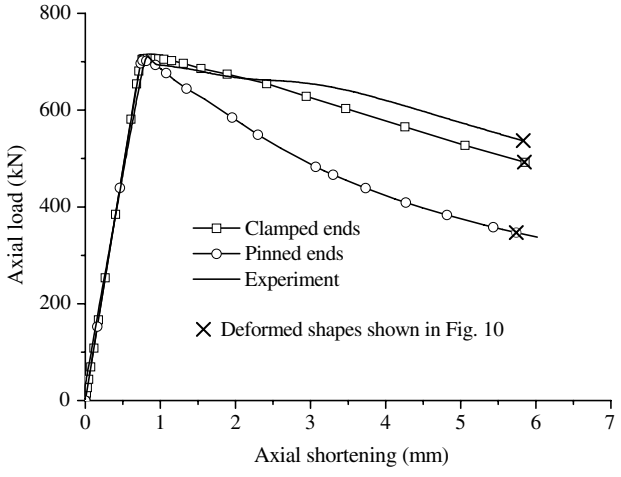


Fig. 9. Load–axial shortening curves of the bare steel tube with different boundary conditions.

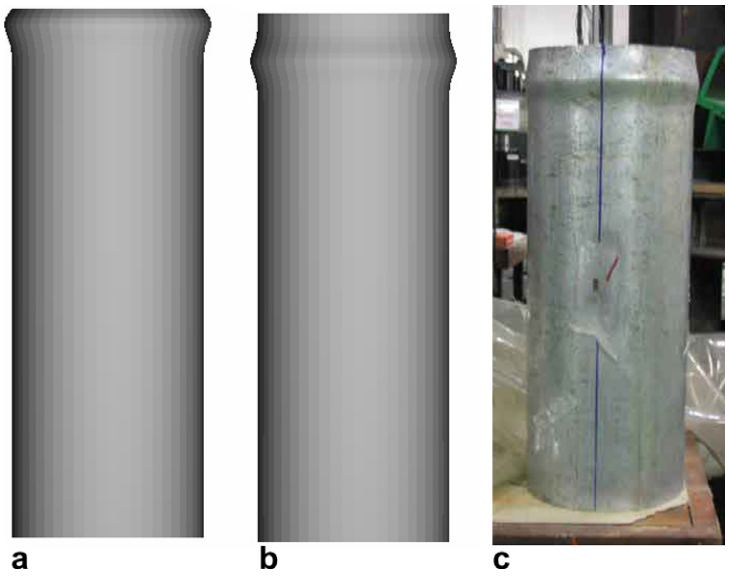


Fig. 10. Failure modes of the bare steel tube with different boundary conditions. (a) FE analysis, pinned ends. (b) FE analysis, clamped ends. (c) Experiment.

the finite element model with two clamped ends, an axisymmetric outward imperfection in the form of a half-wave sine curve along the meridian (i.e. a local outward bulge) was added near one end of the tube and centred at the position of maximum radial displacement from a linear elastic analysis. In the finite element model with pinned ends, the same half-wave imperfection was made to start at the support. The half-wave length of the sine curve was $1.728\sqrt{Rt}$(31.75 mm), where $R$ is the radius of the tube middle surface and t is the tube thickness. This value is equal to the critical half-wave length for the classical axisymmetric elastic buckling mode of axially-compressed cylinders [11]. The imperfection amplitude adopted was 0.02 mm. Such a small local axisymmetric imperfection has little effect on the load–axial shortening behaviour, except that it provided the necessary disturbance to guide the steel tube into the development of only a single local buckle at one of the two ends. Values smaller than 0.02 mm were also tried and were not found to be successful in guiding the tube into the desired pattern of deformation.

## 4. Finite element modelling of FRP-confined steel tubes

The FRP jacket was modelled using beam elements oriented in the hoop direction, which means that the small stiffness of the FRP jacket in the meridional direction was ignored in the finite element model. Each beam element was assigned a narrow rectangular section, with its section width being equal to the nominal thickness of the FRP jacket and its section height being the distance from the mid-height of the shell element above to that of the shell element below the beam element. Element B33 in ABAQUS [15] was used, which is a two-node cubic beam element with six degrees of freedom (three translations and three rotations) per node. FRP was treated as a linear elastic material. The nodes of the beam elements (FRP) formed a node-based surface, which was regarded as the slave surface, and were tied to the shell surface (the steel tube) which was regarded as the master surface. The tensile rupture behaviour of the FRP was not included in the model, but strains developed in the FRP jacket can be compared with the ultimate tensile strain of the FRP from tensile tests to see whether local rupture is predicted.

Similar to the bare steel tube, a geometric imperfection was included in the finite element model for FRP-confined steel tubes to match experimental observations. Ideally, the geometric imperfections should be precisely surveyed and modelled, as has been done in research on much thinner shells [16,17], but even when such an approach is followed for geometric imperfections, the effects of material imperfections such as residual stresses from cold bending [18] are still not included. In the present study, a much simpler approach was adopted. The failure modes of FRP-confined steel tubes (Fig. 5) are no longer axisymmetric and inward buckling deformations away from the two ends are important. To guide the tube into such deformations, a non-axisymmetric geometric imperfection was included in the finite element model for FRP-confined steel tubes. The shape of the imperfection was assumed to be of the following form (Fig. 11):

$$w = w_0 \sin\left(\frac{\pi y}{L}\right)\cos n\theta \tag{1}$$

where $y$ is the axial coordinate from one end of the tube, $\theta$ is the circumferential angle (radian), $w_0$ is the amplitude of the imperfection, $L$ is the half-wave length of the imperfection in the meridional direction, and $n$ is the number of circumferential waves of the imperfection.

Figs. 12–14 show the results of a series of finite element simulations where the effects of varying three parameters are illustrated. It is found that, the finite element predictions are sensitive to the chosen imperfection parameters only in the final stage of deformation (the descending part of the load–axial shortening curve); within the ranges examined, the finite element results match the experimental results closely for all three specimens when the three parameters are: $w_0 = 0.01$ mm, $n = 2$, and $L = 1.728\sqrt{Rt}(31.75$ mm). The final imperfection is a very small imperfection describing sectional ovalization, with a meridional half-wave length being that of the classical axisymmetric buckling mode. This imperfection, although derived from numerical corroboration, can be realistically expected to exist in such steel tubes. The choice of a geometric imperfection for the finite element model of an FRP-confined steel tube with a more rational basis is an issue that requires further investigation.

Each FRP jacket included an overlapping zone and within this overlapping zone, the FRP jacket was thicker. Two alternative treatments of this overlapping zone were explored: (a) the additional thickness of the overlapping zone of 150 mm was directly included in the finite element model; (b) the additional thickness of the overlapping zone was smeared around tube. In both options, the additional ply is taken to be completely effective, which is an optimistic treatment as part of this ply is unlikely to be effective due to the need for stress transfer between plies. Option (a) was used in all simulations presented in Figs. 12–14. For option (b), the smeared equivalent thicknesses of the single-, two- and three-ply FRP jackets are respectively, 0.22 mm, 0.37 mm and 0.53 mm. Fig. 15 shows the test results in comparison with the finite element predictions for the two different modelling options for the overlap. It is seen that the finite element results from the two options are very close to each other except for the one-ply jacket where a significant difference is seen following the attainment of the peak load.

The finite element failure modes of the FRP-confined steel tubes from option (a) are shown in Fig. 16. These deformed shapes are for an advanced state of deformation

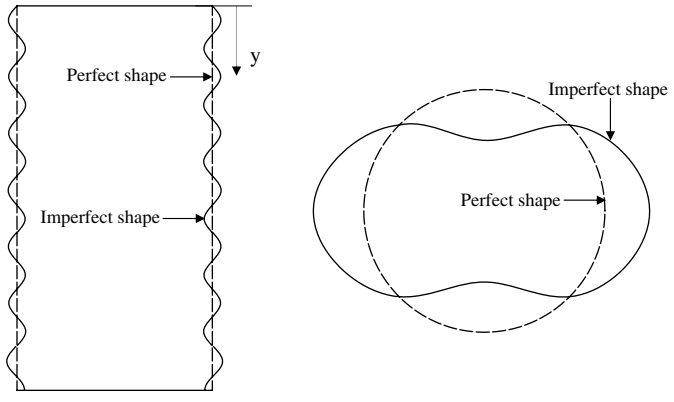


Fig. 11. Imperfection assumed for the FRP-confined steel tubes.

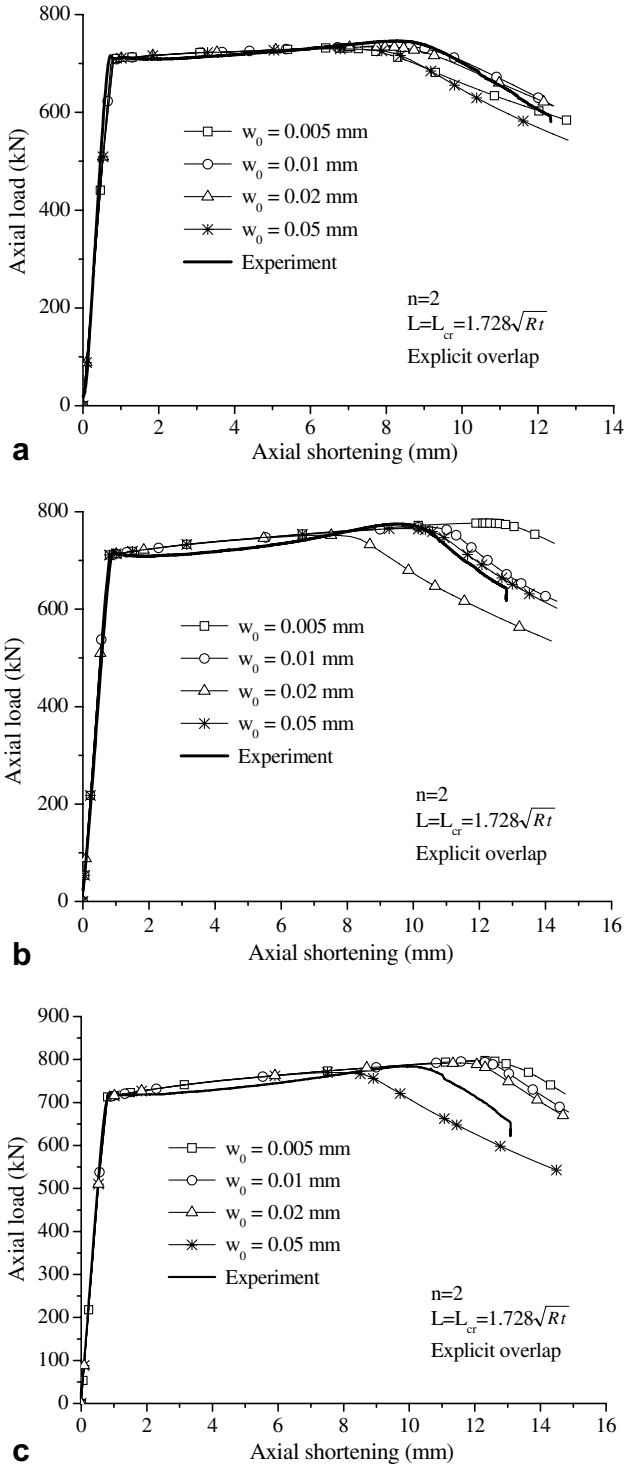


Fig. 12. Effect of imperfection amplitude on load–axial shortening curves: (a) Tube ST-F1, (b) Tube ST-F2 and (c) Tube ST-F3.

corresponding closely to the end of the test (Fig. 15). They match those from the tests reasonably well, given the well-known fact that the buckling mode of a real imperfect axially compressed cylindrical shell is notoriously difficult to predict precisely even when the geometric imperfection is

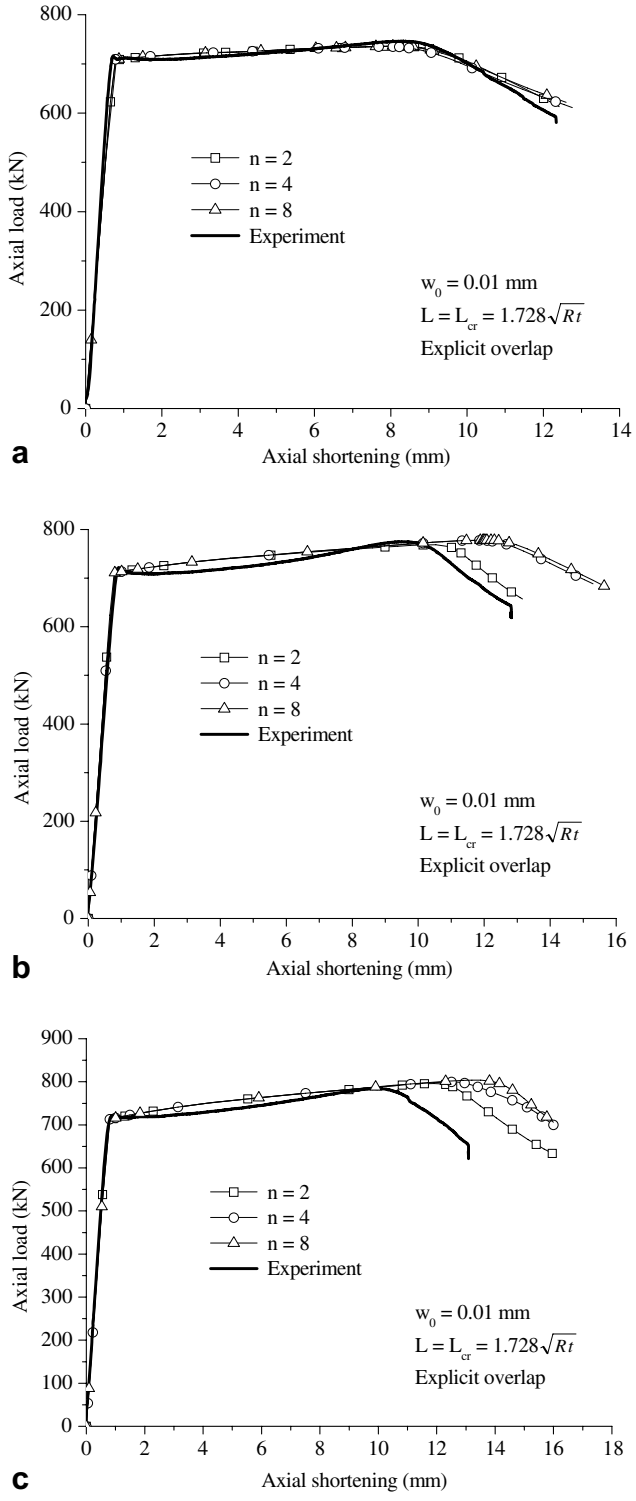


Fig. 13. Effect of circumferential wave number on imperfection on load–axial shortening curves: (a) Tube ST-F1, (b) Tube ST-F2 and (c) Tube ST-F3.

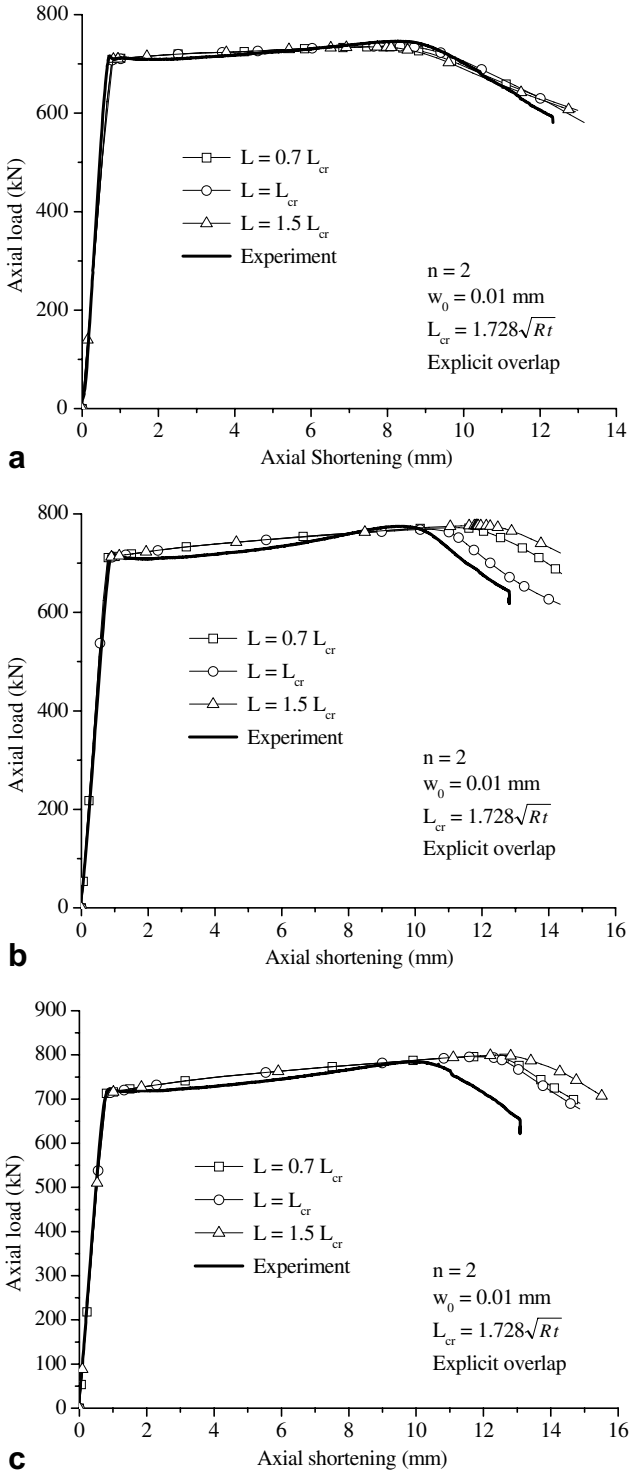


Fig. 14. Effect of meridional half wavelength of imperfection on load–axial shortening curves: (a) Tube ST-F1, (b) Tube ST-F2 and (c) Tube ST-F3.

accurately surveyed and included into the finite element model. For the steel tube confined with a single-ply FRP jacket, the experimental failure mode was primarily outward buckling around the circumference near one of the ends. The finite element model showed that at the ultimate load, the hoop strains in the jacket at the crest of the elephant's foot buckle are higher than those elsewhere and reach mean values of around 0.028 and 0.025 for options

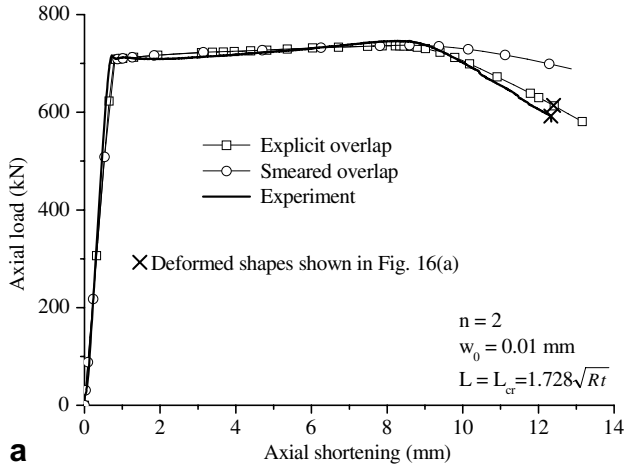


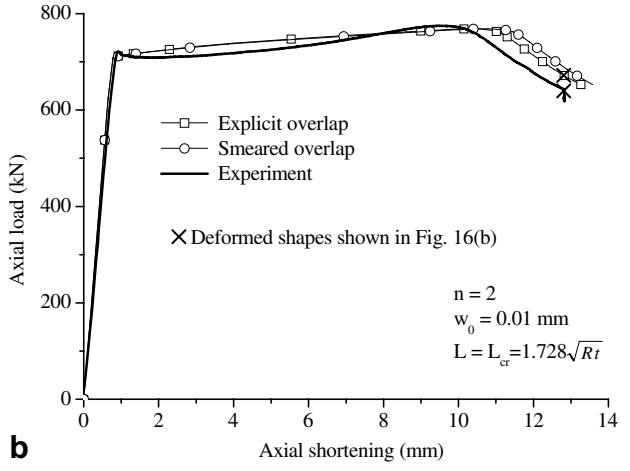


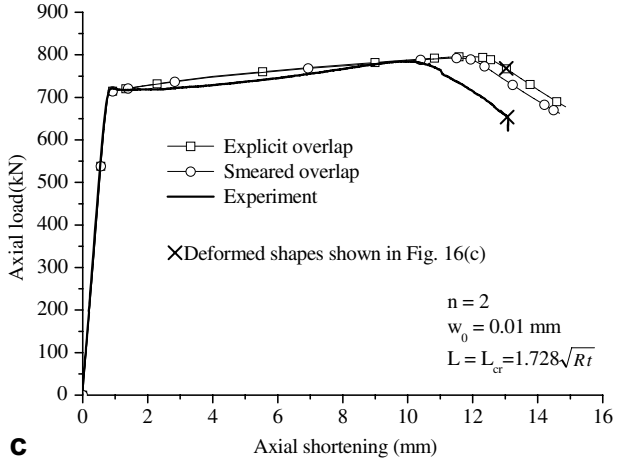


Fig. 15. Load–axial shortening curves of FRP-confined steel tubes: explicit overlap versus smeared overlap: (a) Tube ST-F1, (b) Tube ST-F2 and (c) Tube ST-F3.


Fig. 16. Failure modes of FRP-confined steel tubes: finite element analysis versus experiment: (a) Tube ST-F1, (b) Tube ST-F2 and (c) Tube ST-F3.

(a) and (b). These values are higher than the ultimate strain obtained from tensile tests (0.0228), indicating that in the experiment, local rupture may have been reached before the attainment of the peak load. However, in the experiment, the maximum value of the hoop strain of the jacket detected was only around 0.012 and this is because FRP rupture did not occur at the mid-height of the tube where the strain gauges were located. It should be noted that based on existing research on FRP jackets confining con-

crete cylinders [19,20], the ultimate hoop rupture strain achievable in a circular jacket may be significantly lower than the coupon test result (0.0228) due to the detrimental effect of curvature, although the present tests did not provide enough information to either confirm or refute this observation.

For the steel tubes confined with two-ply and three-ply FRP jackets, respectively, the finite element results showed the hoop strains in the FRP jacket at the ultimate load are not uniformly distributed and high values of hoop strains exceeding 0.0228 in the jacket are highly localised. Hoop strains both near the ends and at the mid-height of the tube are generally below 0.017 at the attainment of the ultimate load, which is closer to the values recorded by strain gauges at the mid-height for both tubes (both around 0.013). These results confirm that in these two specimens, inward buckling deformations were much more important.

Since the tie constraint was adopted to model the interaction between the FRP jacket and the steel tube in the present finite element model, the possibility of debonding between the FRP jacket and the steel tube when the steel tube buckles inward was not considered. Since debonding did occur in the test of the steel tube confined with a three-ply FRP jacket, the use of tie constraint is believed to be the main cause for the significant difference between the finite element and the test load–shortening curves in the descending branch for the two-ply and three-ply jackets (Fig. 15b and c).

It should be noted that when the overlap is directly modelled, the thicker overlapping zone represents a disturbance to the axisymmetry of the tube geometry. In such a case, the use of a non-axisymmetric imperfection is unnecessary to guide the tube into non-axisymmetric buckling deformations. This option was not adopted in the present study as the same non-axisymmetric imperfection given by Eq. (1) was used in all finite element models for FRP-confined steel tubes to facilitate easy comparison.

## 5. Strengthening of thin cylindrical shells against local collapse

It is well known that large thin steel cylindrical shells such as liquid storage tanks and steel silos for storage of bulk solids may fail in the elephant's foot buckling mode when subjected to the combined action of axial compression and internal pressure (Fig. 1) [10,11]. Many such failures have been observed during earthquakes. The idea of FRP jacketing is extended to the strengthening of thin circular cylindrical shells in this section.

In order to demonstrate the strengthening effect of FRP, a bare thin cylindrical shell and three FRP-confined thin cylindrical shells under the combined action of axial compression and internal pressure were analysed using finite element models similar to those developed for steel tubes presented above. The main difference is that the radius is now much larger and an internal pressure exists in addition to axial compression. The radius and thickness of this cylindrical shell are 10,000 mm and 10 mm, respectively. The height of this cylindrical shell is 1543 mm which is twice the linear elastic meridional bending half-wave length ($2 \times 2.44 \times \sqrt{Rt}$), where $t$ and $R$ are the thickness and the radius of the middle surface of the cylindrical shell [11]. The axial compression and the internal pressure have a fixed ratio ($\sigma/p = R/t$).The steel is assumed to be elastic-perfectly plastic with an elastic modulus of 200 GPa and a yield stress of 250 MPa.

Only axisymmetric collapse was considered, so a one-degree axisymmetric model was adopted in the analysis to save computational time. The bottom end of the shell is simply-supported (ie only meridional rotations are allowed). The top end is allowed to move radially and axially but is restrained against meridional rotations. These boundary conditions mean that local buckling can only occur at the base, so the inclusion of an imperfection to guide the shell into a single buckle at the base is not needed.

Three commercially available FRP systems were examined, including the GFRP system (System I) used in the axial compression tests on steel tubes presented earlier in the paper. The other two systems are CFRP systems and the properties given by the suppler were used in the finite element analyses. System II is a normal modulus CFRP system with an elastic modulus of 230 GPa, a tensile strength of 3450 MPa and a nominal thickness of 0.17 mm. The corresponding values for system III, which is a high modulus CFRP system, are 640 GPa, 2560 MPa and 0.19 mm. In each case, the shell is wrapped with a 10-ply jacket. The four axial stress-shortening curves from finite element analyses are shown in Fig. 17. It can be seen that the ultimate load increases with increases in the elastic modulus of the FRP as can be expected. The failure mode (Fig. 18) remains similar in shape but the length of the buckle reduces with increases in the elastic modulus of the FRP. It can be concluded that FRP confinement provides an effective method for the strengthening of steel cylindrical shells against local collapse failure.

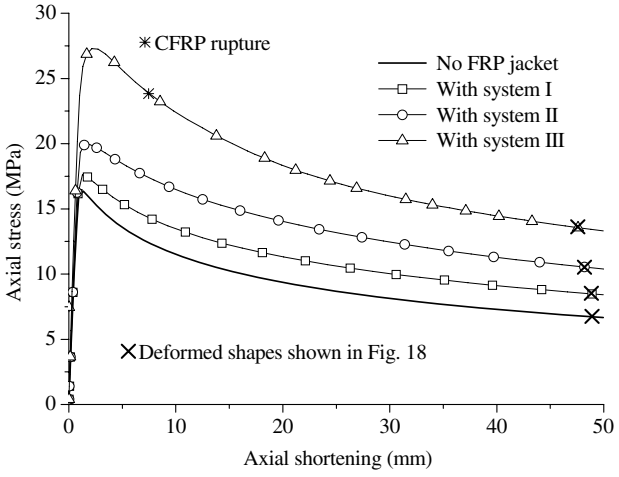


Fig. 17. Axial stress-shortening curves of pressurized thin cylindrical shells under axial compression.

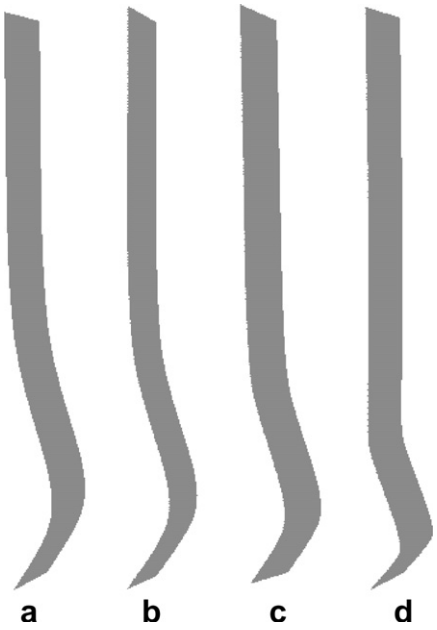


Fig. 18. Failure modes of pressurized thin cylindrical shells under axial compression. (a) No FRP jacket, (b) With system I and (c) With system II (d) With system III.

## 6. Conclusions

In this paper, the use of FRP confinement to enhance the ductility and hence the seismic resistance of circular steel tubes has been explored. A series of axial compression tests has been presented to demonstrate the effectiveness of FRP confinement of steel tubes whose ductility is otherwise limited by the development of the elephant's foot buckling mode. A finite element model for predicting the behaviour of these FRP-confined tubes has also been presented. Both the load–axial shortening curves and the failure modes from the finite element model are in close agreement with those from the tests, although the degree of accuracy depends significantly on the geometric imperfection included in the finite element model. The choice of geometric imperfections in the finite element model for FRP-confined steel tubes is an issue that requires further investigation in the future. Both test and numerical results have shown conclusively that with the provision of a thin FRP jacket, the ductility of the steel tube can be greatly enhanced. These results have also shown that when the jacket thickness reaches a threshold value for which inward buckling deformations dominate the behaviour; further increases in the jacket thickness do not lead to significant additional benefits as the jacket provides little resistance to inward buckling deformations. It is significant to note that FRP confinement of steel tubes leads to large increases in ductility but limited increases in the ultimate load, which is desirable in seismic retrofit so that the retrofitted tube will not attract forces which are so high that adjacent members may be put in danger.

The use of FRP jackets to strengthen thin steel cylindrical shells against local elephant's foot buckling failure at the base has also been explored through finite element analyses. The limited numerical results for a thin cylindrical shell with a radius-to-thickness ratio of 1000 and subjected to axial compression in combination with internal pressure indicate that the method leads to significant increases of the ultimate load. If this method is used in seismic retrofit, a gap between the steel shell and the FRP jacket should be considered [7] so that the FRP jacket leads to only limited increases in the ultimate load but still large increases in the energy absorption capacity. The FRP jacketing of steel cylindrical shells can also be used in the construction of new tanks and silos to enhance their performance.

## Acknowledgements

The authors are grateful to the Research Grants Council of Hong Kong (B-Q932) and The Hong Kong Polytechnic University (1ZE-06 and RGU4) for their financial support.

## References

[1] Teng JG, Chen JF, Smith ST, Lam L. FRP strengthened RC structures. John Wiley & Sons Ltd; 2002.
[2] Teng JG, Chen JF, Smith ST, Lam L. Behaviour and strength of FRP-strengthened RC structures: a state-of-the-art review. Proc Inst Civil Eng–Struct Build 2003;156(SB1):51–62.
[3] Hollaway LC, Cadei J. Progress in the technique of upgrading metallic structures with advanced polymer composites. Prog Struct Eng Mater 2002;4:131–48.
[4] Kitada T, Yamaguchi T, Matsumura M, Okada J, Ono K, Ochi N. New technologies of steel bridges in Japan. J Construct Steel Res 2002;58(1):21–70.
[5] Teng JG, Hu YM. Enhancement of seismic resistance of steel tubular columns by FRP jacketing. In: Proceedings, 3rd international conference on composites in construction, Lyon, France; 11–13 July 2005.
[6] Xiao Y. Application of FRP composites in concrete columns. Adv Struct Eng 2004;7(4):335–41.
[7] Xiao Y, He WH, Choi KK. Confined concrete-filled tubular columns. J Struct Eng, ASCE 2005;131(3):488–97.
[8] Teng JG. and Hu YM. Suppression of local buckling in steel tubes by FRP jacketing. In: Proceedings, 2nd international conference on FRP composites in civil engineering, Adelaide, Australia; 8–10 December 2004.
[9] Nishino T. and Furukawa T. Strength and deformation capacities of circular hollow section steel member reinforced with carbon fiber. In: Proceedings of 7th Pacific structural steel conference, American Institute of Steel Construction; March 2004.
[10] Rotter JM. Local collapse of axially compressed pressurized thin steel cylinders. J Struct Eng, ASCE 1990;116(7):1955–70.
[11] Rotter JM. Chapter 2: cylindrical shells under axial compression. In: Teng JG, Rotter JM, editors. Buckling of thin metal shells. UK: Spon Press; 2004. p. 42–87.
[12] Teng JG. Plastic collapse at lap-joints in pressurized cylinders under axial load. J Struct Eng, ASCE 1994;120(1):23–45.
[13] BS 18. British standard method for tensile testing of metals. British Standard Institution; 1987.
[14] ASTM3039. Standard test method for tensile properties of polymer matrix composite materials. American Society for Testing of Materials; 2000.

[15] ABAQUS, ABAQUS/Standard User's Manual. ABAQUS Inc; 2003.
[16] Zhao Y, Teng JG. Buckling experiments on cone-cylinder intersections under internal pressure. J Eng Mech, ASCE 2001;127(12):1231–9.
[17] Teng JG, Lin X. Fabrication of small models of large cylinders with extensive welding for buckling experiments. Thin-Walled Struct 2005;43(7):1091–114.
[18] Quach WM, Teng JG, Chung KF. Residual stresses in steel sheets due to coiling and uncoiling: a closed form analytical solution. Eng Struct 2004;26(9):1249–59.
[19] Lam L, Teng JG. Ultimate condition of FRP-confined concrete. J Comp Construct, ASCE 2004;8(6):539–48.
[20] Teng JG, Lam L. Behavior and modeling of FRP-confined concrete. J Struct Eng, ASCE 2004;130(11):1713–23.